Proceedings of ASME Turbo Expo 2024
Turbomachinery Technical Conference and Exposition
GT2024
June 24-28, 2024, London, United Kingdom

GT2024-125360

NASA HECC GEOMETRY AND PERFORMANCE REVIEW PART 2: GEOMETRIC DIFFERENCES BETWEEN THE AS-MANUFACTURED AND DESIGN-INTENT IMPELLER GEOMETRY AND THEIR EFFECTS ON THE VANELESS DIFFUSER CONFIGURATION PERFORMANCE

Gregorio Robles Vega[1], Alec J. Bosshart[1], Michael Ni[1], Ron-Ho Ni[1], Herbert M. Harrison[2], Tammy Nguyen-Huynh[2,3]

[1]AeroDynamic Solutions Inc, San Ramon, CA
[2]NASA Glenn Research Center, Cleveland, OH
[3]The Ohio State University, Columbus, OH

ABSTRACT

An investigation of the NASA High Efficiency Centrifugal Compressor (HECC) vaneless diffuser configuration was performed. This multipart investigation focused on validating the computational model against experimental data. The validated model was then used to explore the effects of observed geometric differences between the As-Manufactured and Design-Intent impellers. Lastly, the validated model was used for comparison against an experimental tip clearance study.

Part II of the investigation of the NASA HECC vaneless diffuser configuration focused on understanding the differences in geometry and performance between the As-Manufactured impeller and the Design-Intent impeller. This was achieved through comparison of the As-Manufactured HECC vaneless computational model, developed from the solid model of the impeller and validated in Part I, against a new model developed from the Design-Intent blade sections published in NASA/CR-2014-218114/Rev1. The 1D performance values showed that the As-Manufactured impeller underperformed compared to the Design-Intent for all four speedlines that were simulated. Further investigation of profiles, loading and contours showed consistent underperformance of the As-Manufactured relative to the Design-Intent. An investigation into the source of the performance differences led to the discovery of several significant variations in the impeller geometries. The differences that were observed can be summarized into four categories: fillets, trailing-edge exit radii variation, dissimilarity in the splitter leading-edge geometry and main blade thickness differences. The investigation then shifted its effort to quantify the performance effects caused by geometric differences. The investigation showed that out of the four geometric differences that were explored, the differences in the splitter blade had the largest impact. These differences most notably changed flow physics near the splitter leading edge, especially near the tip of the impeller.

NOMENCLATURE

GPU	Graphics Processing Units
TPR	Total Pressure Ratio
TTR	Total Temperature Ratio
LE	Leading Edge
TE	Trailing Edge
R	Radial Coordinate
RT	Circumferential Coordinate (R*Theta)
η	Isentropic Efficiency
γ	Ratio of Specific Heats
M_{U_2}	Machine Mach Number
U_2	Physical Speed of Trailing Edge Radius

1. INTRODUCTION

Numerical models, from simple 1-D design codes to advanced 3-D, time-resolved simulations, require major investments of time, care and experience to achieve accurate representations of the actual flow fields in turbomachines [1]. This is due to the amalgamation of flow phenomena present within turbomachinery flows that present problems for current turbulence modeling techniques: adverse pressure gradients, transition regions, flow path curvature, high levels of mixing, and changing references frames are all part of the processes required to impart or extract work to and from the flow [2,3].

Since these fluid phenomena are inherent to turbomachines, care must then be taken in all other aspects of the model to assure that the in-built challenges of flow prediction are not exacerbated by inaccuracies in the model of the hardware. For example, bleed cavities and leakage paths are almost always present, but are often neglected due to the relatively low impact on overall stage performance paired with the high computational cost needed to include them in the model [4–6]. Rotor and stator fillets are also often neglected due to the complications they add to the gridding

process [7]. These choices are acceptable, but the simplifications made to the geometry must be justified and accounted for to ensure the modeling choices do not lead to unexpected outcomes in the final numerical results.

Of utmost importance, however, is ensuring that the numerically modeled geometry accurately reflects the physical hardware. While this may seem an overly apparent assertion, the process to arrive at the physical hardware from the design process is laborious. The final geometry output from the design phase is usually the desired shape at "hot conditions" – the design point at which the machine is under load. A hot-to-cold transformation process must be conducted to provide the geometry which must be machined, and the coordinates exported through various formats resulting in a final file that can be utilized in the fabrication process [8]. Regardless, if the final physical hardware is not an accurate reflection of the intended design, numerical prediction of the flow will not capture the reality.

The NASA High Efficiency Centrifugal Compressor (HECC) is one of a select few open-source centrifugal compressor designs that have the required geometry and experimental data necessary for CFD code validation. This dataset was further expanded by the release of the HECC vaneless diffuser configuration geometry and experimental data by Harrison et al [9,10]. Moreover, the removal of the vaned diffuser and exit guide vane from the configuration provided an opportunity to focus on the impeller performance in isolation from the vaned diffuser. Thus, this multipart investigation is focused on this configuration.

The present part of the multipart study explores the efficacy of the Design-Intent geometry of the HECC impeller compared to that of the As-Manufactured geometry. Previously in Part 1, the As-Manufactured numerical model of the HECC vaneless configuration was extensively validated against the physical hardware and experimental results with satisfactory results. The simulated impeller geometry was confirmed to accurately represent the physical hardware via inspections and coordinate measuring machine, and the numerical simulations predicted the impeller and stage performance with accuracy satisfactory for detailed investigation into the flow field. The As-Manufactured and Design-Intent models of the HECC impeller will now be compared in this second part of the three-part paper series to understand the differences between the two. It should be noted that the expectation was for this comparison to be an additional verification of the model and that the Design-Intent impeller geometry would match the As-Manufactured. The only differences that were expected to be observed were thought to be explainable by cold-to-hot transformation differences. However, during the execution of the investigation it was found to not be the case. These observed differences in geometry and their effects on the performance are the focus of the following sections.

2. HECC VANELESS STAGE AND INSTRUMENTATION

The experimental data obtained for validation of the computational model in the present work were conducted at NASA Glenn Research Center using the High Efficiency Centrifugal Compressor vaneless diffuser configuration. The major components and instrumentation in the stage relevant for aerodynamic measurements are presented in Figure 1. The primary flow path is composed of the stage inlet, impeller, and vaneless diffuser. After the radial-to-axial bend, the flow is passed to a collector, through a throttle valve, and exhausted to the atmosphere. The impeller has 15 main blade/splitter blade pairs, and the diffuser is entirely vaneless through both its radial and axial portions. The impeller design speed is 21,789-rpm at standard day conditions. At the design mass flow rate of 11-lbm/s, the impeller total pressure ratio is 5.11 and the stage total pressure ratio is 4.54. The machine Mach number (1) is approximately 1.45 at design conditions.

$$M_{U_2} = \frac{U_2}{\sqrt{\gamma R T_{00}}} \tag{1}$$

The design intent tip clearance is 2.0% of the exducer blade height, or 0.012-in. Extensive documentation on the experimental measurements in the HECC have been provided by Medic et al. [7] and Harrison et al. [9,10].

Compressor steady performance metrics are acquired in the compressor inlet settling chamber (Station 0), at the impeller exit (Station 3), and the stage exit (Station 7) with total temperature and total pressure rakes, Figure 1. Cobra-style three-hole probes and total temperatures probes are also traversed across the span at Station 3 to characterize the impeller exit flow in greater detail than is possible with stationary rakes. Finally, static pressure taps are distributed throughout the flow path of the stage. Further details on the instrumentation available in the vaneless diffuser configuration are given in Part 1 of this paper and by Harrison et al. [9].

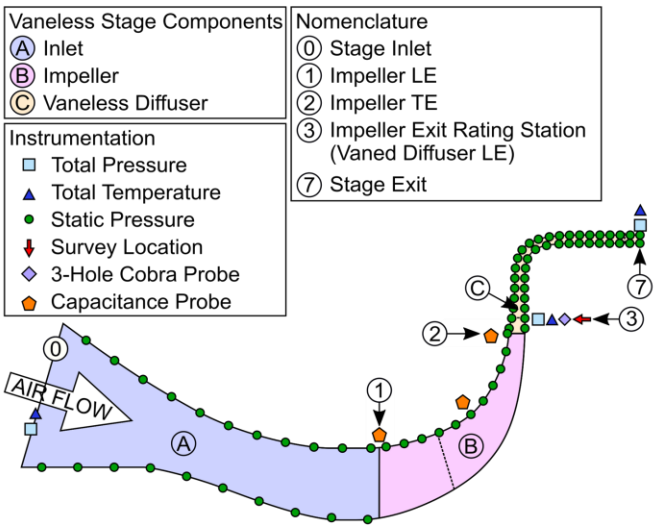

FIGURE 1: HECC VANELESS DIFFUSER COMPONENTS, NOMENCLATURE, AND INSTRUMENTATION

3. COMPARISON TO DATA

3.1 Modeling Approach

The same model configuration was used for all the numerical simulations in all three parts of the present study. This was done so that any conclusions would be clearly attributed to the impeller geometry differences being explored rather than differences in the mesh counts or flow solver settings. Thus, a thorough validation effort was undertaken in part 1 using sections extracted from the CAD geometry made publicly available in 2023 [10]. This CAD geometry was confirmed to match the manufactured impeller with a coordinate measuring machine. The section data extracted from the CAD impeller geometry, which included the fillets definition in the coordinates, were thereafter referred to as the As-Manufactured impeller geometry. Part 1 detailed a mesh convergence study that was conducted. Brief details regarding this study can be found in section 3.1.1. The solver settings used for the validation include the use of the Wilcox kw 98 turbulence model and wall integration. A detailed description of the solver settings can be found in Part 1 and summarized in section 3.1.2.

In the present part the same mesh counts and solver settings were used. The only changes in the model are the impeller coordinates. In the present paper the focus shifted to a comparison of the As-Manufactured impeller geometry against the original geometry published by Medic et al [7], referred to as the Design-Intent impeller geometry. The expectation was that these geometries would only contain differences in geometry from a hot-cold process. However, as part of the study it was discovered that there were differences between the As-Manufactured and Design-Intent geometries that were of a magnitude not explainable by a hot-cold process. It should be noted that the difference between the As-Manufactured and Design-Intent was only possible due to the release of the CAD model part in 2023 by Harrison et al [9,10] and the verification that the manufactured impeller in the rig matched the CAD model. After the differences between the geometries and their effect on the performance were quantified, the present paper shifts to providing an overview of the effect of the various geometric differences discovered. For all these simulations the model configuration remained the same with the only change being the impeller coordinates.

3.1.1 Design-Intent Mesh

As described in Section 3.1, the mesh settings were kept constant between the As-Manufactured and Design-Intent models. The meshes were generated using a commercially available structured multiblock mesh generator, Code Wand. A detailed mesh convergence study can be found in Part I. It consisted of four mesh levels each run at 8 points along the speedline. The study showed the Fine mesh had achieved mesh independence at all points along the speedline. The mesh counts for the Fine mesh level were used for both the As-Manufactured and Design-Intent simulations. They are as follows: 45 radial planes across the span, 17 radial planes in the tip mesh, 249 points around the main blade, and 169 points around the splitter blade. In total, this mesh configuration yields a full stage that contains 2,027,603 nodes and 1,991,968 elements. A constant tip clearance of 0.012-in was used. The mesh can be seen below in Figure 2.

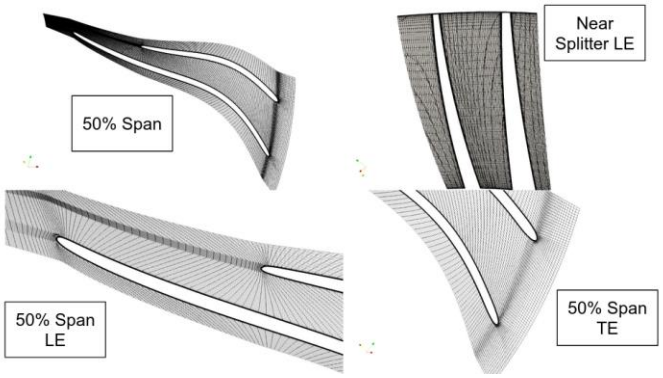

FIGURE 2: DESIGN INTENT MESH

3.1.2 Design-Intent Solver Settings

The solver used for the multipart investigation was the GPU accelerated Code Leo solver. Code Leo is a commercially available density-based, compressible flow solver [12]. The Design-Intent simulations were executed using the same solver settings as the As-Manufactured model validation in Part I. These settings include an inlet total pressure and total temperature of 14.7 psi and 518.7°R. Similarly, both models used the Wilcox K-ω 98 turbulence model with a variable ratio of specific heats.

Both the As-Manufactured model from part I and the present simulations were executed on a laptop with 1 Nvidia RTX A5000 Mobile GPU on which one simulation would complete 6,000

iterations (typical number of iterations required for convergence) in approximately 7 minutes and 42 seconds.

3.2 Speedline Results

With the previously described model setup, a speedline was created for the Design-Intent geometry. The speedline was generated using an automated, iterative tool that marches the solution towards numerical stall to within 0.1% exit static pressure change. Each case was evaluated for convergence with flow rate, total temperature, total pressure and other performance parameters being monitored. The resulting speedlines can be seen in Figure 3, with the green curve representing the Design-Intent geometry, the red curve representing the As-Manufactured geometry, and the black points showing the experimental results. For Figure 3.C, the stage efficiency is calculated with Equation (2):

$$\eta = \frac{TPR^{\frac{\gamma-1}{\gamma}} - 1}{TTR - 1} \quad (2)$$

It can be immediately observed that the Design-Intent simulations are substantially greater in stage TPR, stage TTR, and stage efficiency relative to the As-Manufactured results. At the design point (11lb_m/sec) the Design-Intent stage pressure ratio and stage efficiency are approximately 0.1 and 1% higher than the As-Manufactured, respectively. The Design-Intent geometry has a slightly lower choke flow rate than the As-Manufactured geometry and also has a larger stall margin. A comparison of the choke flow rate against the experiment cannot be made. Harrison et. al. [9] notes that the maximum mass flow rate in the experiment was limited by the throttle rather than inducer choke. As such, the experiment was able to approach the choke mass flow rate at 100% corrected speed but not reach it.

As previously mentioned, this was not the expected outcome. Originally it was expected that the Design-Intent and the As-Manufactured geometry would have similar performance with any observed differences being attributable to cold-to-hot transformation differences. However, the outcome showed a drastic difference between Design-Intent and As-Manufactured.

To verify that the differences observed at 100% speed also occurred at different off-design conditions, simulations were executed at three other speeds: 105%, 95%, and 90% speeds. It should be noted that the same impeller geometries were used in the off-design conditions. The results from these simulations can be seen in Figure 4. The off-design speedlines again show a significant difference between the As-Manufactured and the Design-Intent models. Since both models were exactly the same at a given rotational speed, except for the impeller geometry, focus shifted to an evaluation of the loading profiles to understand the location along the blade chord where the performance differences arise from.

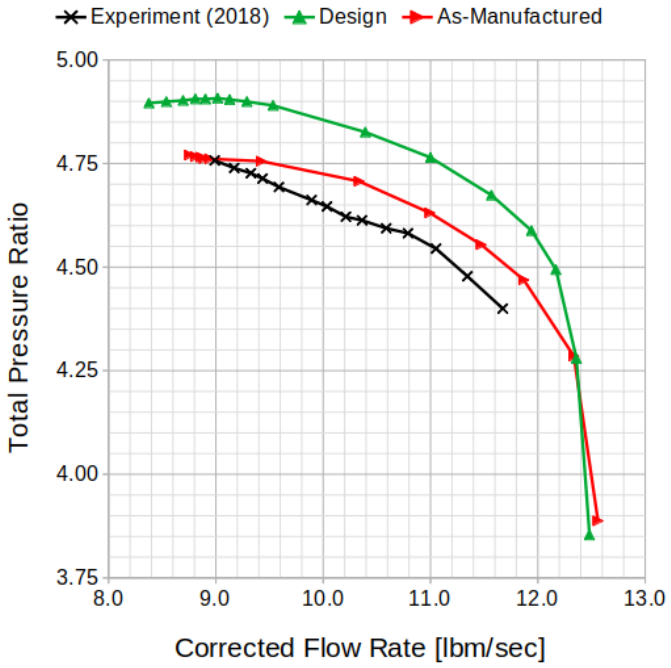

FIGURE 3.A: TPR COMPARISON BETWEEN EXPERIMENTAL DATA (BLACK), AS-MANUFACTURED MODEL (RED), AND DESIGN-INTENT MODEL (GREEN)

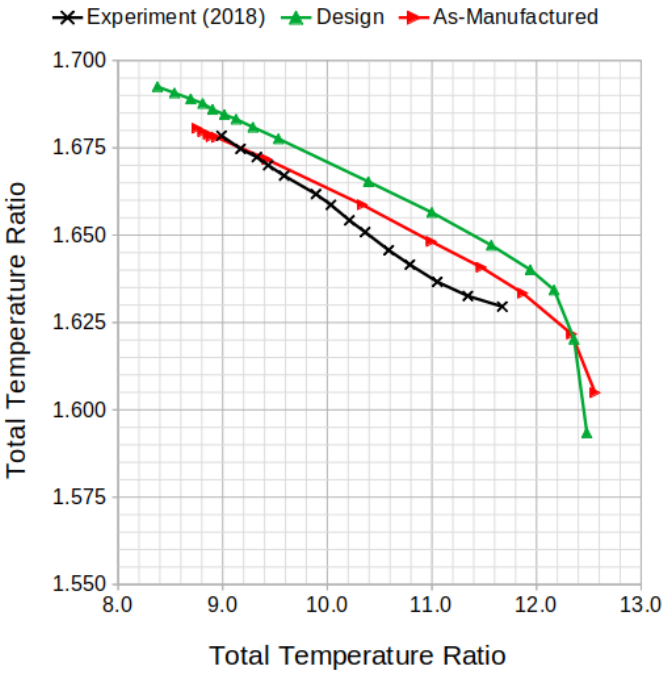

FIGURE 3.B: TTR COMPARISON BETWEEN EXPERIMENTAL DATA (BLACK), AS-MANUFACTURED MODEL (RED), AND DESIGN-INTENT MODEL (GREEN)

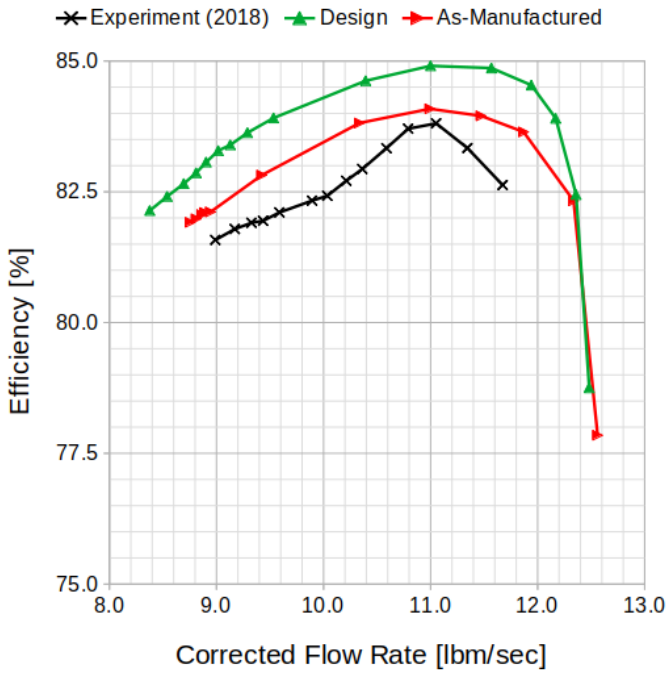

FIGURE 3.C: STAGE EFFICIENCY COMPARISON BETWEEN EXPERIMENTAL DATA (BLACK), AS-MANUFACTURED MODEL (RED), AND DESIGN-INTENT MODEL (GREEN)

To investigate the cause of the difference in the performance of the Design-Intent and As-Manufactured models, the isentropic Mach number along the main and splitter blades of the impeller were plotted for the design point at various spans. It was observed that the loading for the Design-Intent was more ideal than that for the As-Manufactured, shown in Figure 5. The As-Manufactured model showed an overspeed on the splitter blade leading edge. Moreover, the main blade had a drop in work at the same region where the splitter blade leading edge was located while the Design-Intent had no such drop in work at that location. Thus, it highlighted that comparing the splitter blade leading edge for both geometries could reveal more insight into the source of the performance differences.

To further investigate the differences between the models shown in the impeller loading results, flow field contours were created near 70% span, a region where the loading charts showed the most significant difference between the models. Two properties were evaluated: static pressure (Figure 6.A) and relative Mach number (Figure 6.B). The contours reveal drastically different flow fields. In Figure 6.A, the As-Manufactured flowfield shows a notably positive incidence on the splitter. This positive incidence causes a region of much lower static pressure on the splitter suction side near the leading edge. No such phenomenon is seen in the Design-Intent geometry. Further downstream, Figure 6.B shows that the splitter suction side contains an additional low-momentum region that is larger than the one seen in the Design-Intent geometry. This low-momentum region is a source of loss in the machine, and will reduce the stall margin of the As-Manufactured impeller.

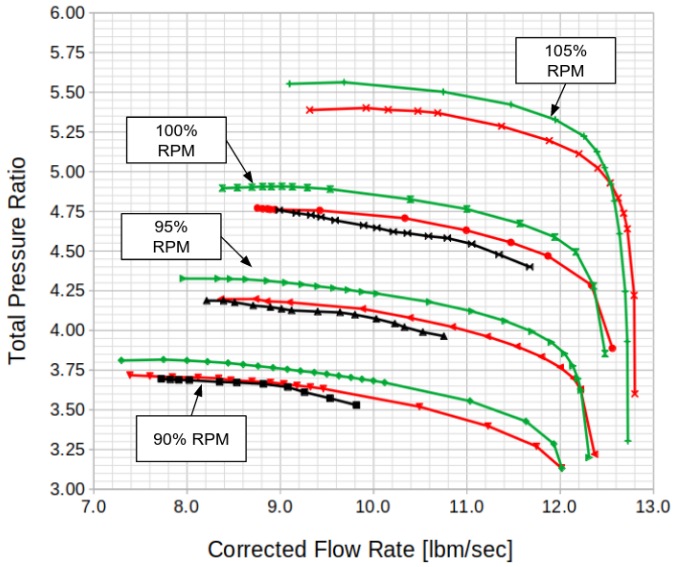

FIGURE 4: OFF-DESIGN TPR COMPARISON BETWEEN EXPERIMENTAL DATA (BLACK), AS-MANUFACTURED MODEL (RED), AND DESIGN-INTENT MODEL (GREEN)

3.3 Impeller Loading Results

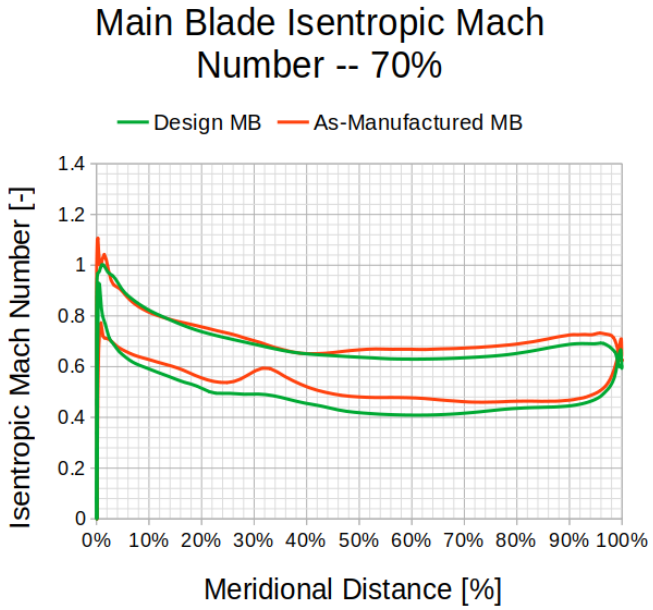

FIGURE 5.A: COMPARISON OF DESIGN-INTENT AND AS-MANUFACTURED MAIN-BLADE 70% SPAN ISENTROPIC MACH NUMBER LOADING AT DESIGN POINT

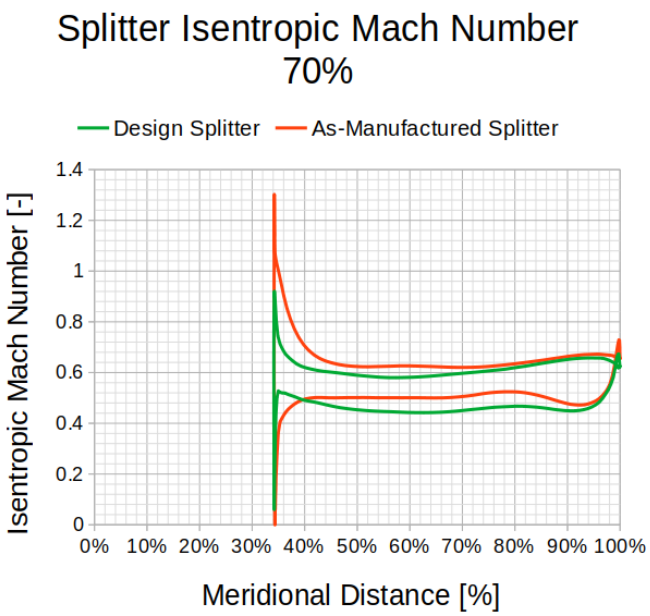

FIGURE 5.B: COMPARISON OF DESIGN-INTENT AND AS-MANUFACTURED SPLITTER-BLADE 70% SPAN ISENTROPIC MACH NUMBER LOADING AT DESIGN POINT

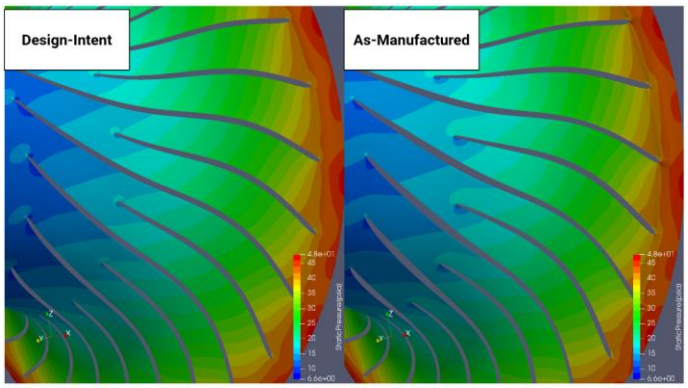

FIGURE 6.A: COMPARISON OF THE STATIC PRESSURE CONTOURS AT 70% SPAN BETWEEN DESIGN-INTENT AND AS-MANUFACTURED MODELS AT THE DESIGN POINT

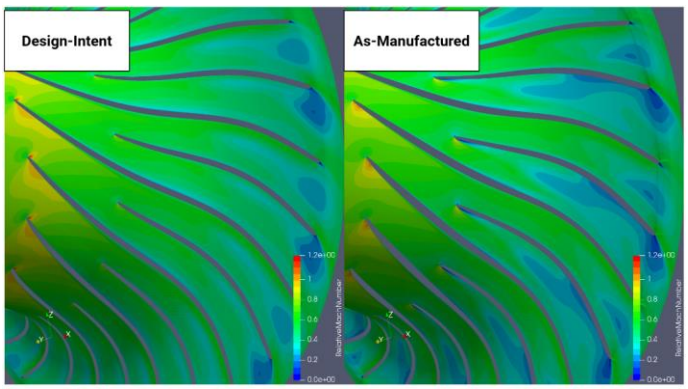

FIGURE 6.B: COMPARISON OF THE RELATIVE MACH NUMBER CONTOURS AT 70% SPAN BETWEEN DESIGN-INTENT AND AS-MANUFACTURED MODELS AT THE DESIGN POINT

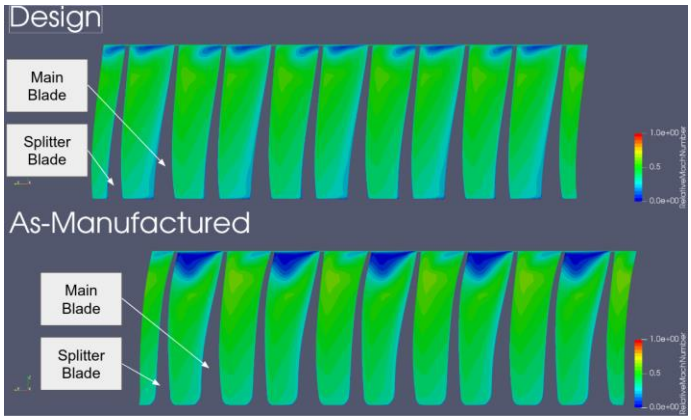

FIGURE 7: SPANWISE VIEW OF FLOWFIELD DOWNSTREAM OF SPLITTER LE

The differences shown between the Design-Intent and As-Manufactured flowfields at 70% span for the peak efficiency point are also shown to exist at additional spans. The flowfields were transformed into meridional space and a slice was taken at the same location in each, slightly downstream of the splitter LE, shown in Figure 7. The Design-Intent geometry shows a tip clearance flow on each side of the splitter blade, and it does not show any other concerning loss mechanisms. The As-Manufactured geometry shows a large low-momentum region occupying approximately 15% of the span near the tip in the passage on the splitter suction side. This region is asymmetric about the splitter, with the pressure side showing a weaker tip clearance flow than the Design-Intent splitter pressure side.

4. DIFFERENCES IN GEOMETRY

The previous discussion on the speedlines, loading, and contour comparisons indicated that the two geometries were performing drastically differently. These differences could only be explained by physical differences in the geometries themselves. Thus, a thorough comparison of the geometry was made.

Four key differences were found: the presence of fillets, differences in the trailing edge radial-coordinate, differences in the placement of the splitter blade leading edge and thickness differences in the main blade. Each of these key differences are described in greater detail in the following subsections.

4.1 Fillets

It was observed that the As-Manufactured geometry has fillets on both the main blade and splitter blade of the impeller (Figure 8). These fillets were not present in the Design-Intent geometry. The inclusion of the fillets into the As-Manufactured section data was intentional. As detailed in Part 1, the As-Manufactured section data was extracted directly from a CAD model that was confirmed to match the manufactured impeller with a coordinate measuring machine. On the other hand, the Design-Intent sections came from the design process and did not include fillets. It should be noted that it is not expected that the fillets will have a major effect on the performance. Rather they

are included first among the list of key geometric differences given the subject matter of the present investigation.

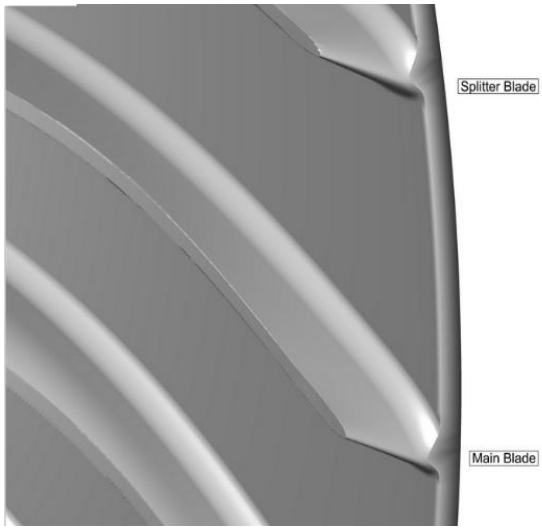

FIGURE 8: AS-MANUFACTURED FILLETS

4.2 Impeller TE Radius

The second geometric difference that was observed was a slight difference in the trailing edge radial-coordinate. The differences in the trailing edge exit radius can be seen in Figure 9 where the two section data are plotted against each other. The Design-Intent geometry can be seen as the green lines, while the As-Manufactured geometry can be seen as the red lines. Figure 9 shows that on average, the TE Radius of the Design-Intent main-blade is approximately 0.014" greater than the As-Manufactured, and 0.016" greater in the splitter.

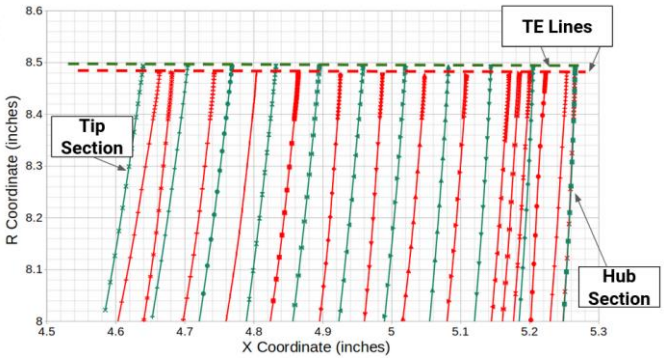

FIGURE 9: AS-MANUFACTURED MAIN BLADE IMPELLER TE LINE (RED) VS. DESIGN-INTENT MAIN BLADE TE LINE (GREEN)

4.3 Splitter Differences

One of the most notable differences between the As-Manufactured and Design-Intent geometries lies in the first quarter of the splitter chord. The Design-Intent splitter geometry has a significant bow in its leading edge, while the As-Manufactured splitter geometry has a straight leading edge, as shown in Figure 10. In Figure 10, the Design-Intent LE can be seen in green, while the As-Manufactured LE can be seen in gray.

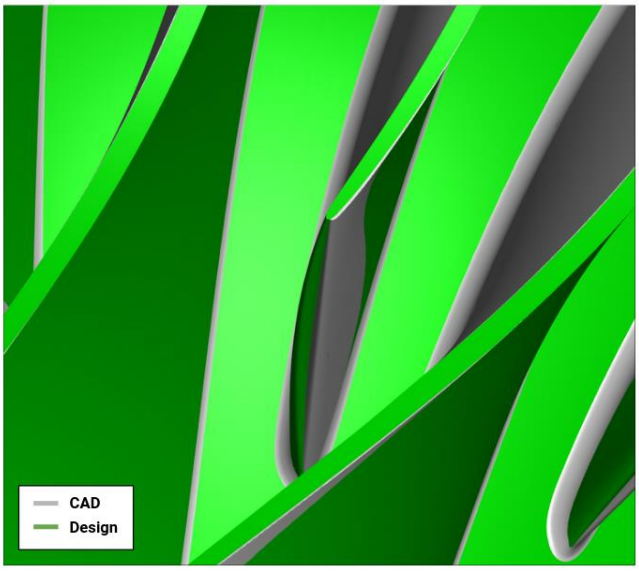

FIGURE 10: DESIGN-INTENT SPLITTER LE GEOMETRY (GREEN) VS. CAD SPLITTER LE GEOMETRY (GRAY)

From this change in the splitter leading edge location, there is a significant change to the camber line and leading edge metal angle for a significant portion of the span. The largest difference in the splitter leading edge location was found to be approximately 0.075-in. For context, the thickness of the splitter leading edge is also approximately 0.075-in. A comparison of the blade profiles at the span where this maximum difference occurs can be seen in Figure 11, where the Design-Intent impeller can be seen as a green surface, and the As-Manufactured blades as red outlines. This surface represents the geometry at approximately 75% span.

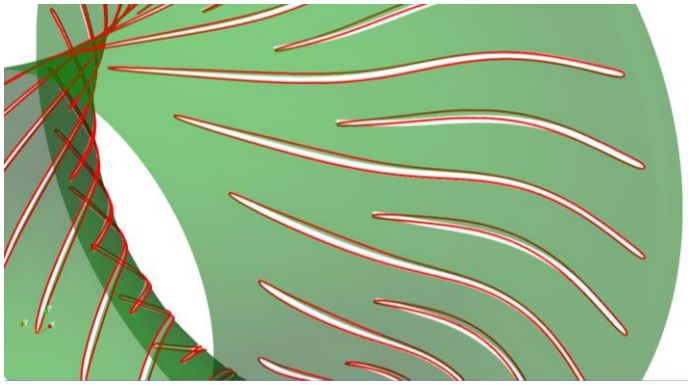

FIGURE 11: DIFFERENCES IN THE IMPELLER CAMBER LINES, 75% SPAN

4.4 Main Blade Differences

Another significant difference in the geometry that can be seen in Figure 11 is the thickness of the main blade. The As-Manufactured impeller main blade is significantly thicker than the Design-Intent impeller main blade. Like the difference in the geometry of the splitter, this difference occurs at multiple spans. To illustrate these differences, Figure 12 shows a constant radius cut of the geometries at a radius 3.8" (approximately midspan of the splitter blade LE). Similar differences were verified to exist at a constant radius cut of 3.0". The Design-Intent geometry is shown in green, and the As-Manufactured geometry is shown in gray. These radial cuts also illustrate that the thickness difference mainly occurs on the pressure side of the main blade. This change to the thickness also causes an adjustment to the overall camber line of the airfoil and the area of the passage on each side of the splitter. A comparison of these differences in the passage area can be seen in Figure 13. In Figure 13, the green lines represent the Design-Intent passage areas, and the red lines represent the As-Manufactured passage areas. For each geometry, a dashed line is used to represent the splitter suction side area, and a solid line is used to represent the splitter pressure side area. The As-Manufactured geometry shows a notably different area distribution between the two passages, especially between Stations 3 and 5. In the As-Manufactured geometry, the main-blade suction side has a much larger passage area than the splitter suction side at Station 3. Moving toward the trailing edge, this phenomenon reverses toward Station 5, where the main-blade suction side area is larger than the splitter suction side area. In comparison, the area in each passage is much closer to equal in the Design-Intent geometry.

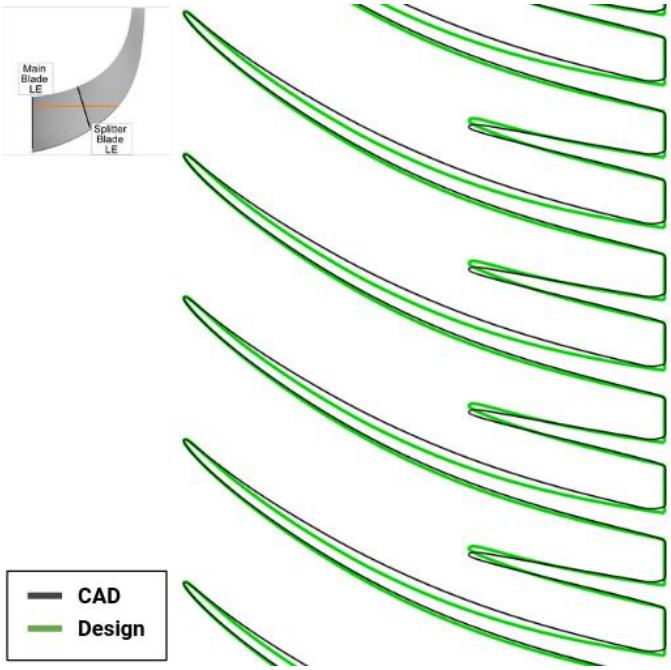

FIGURE 12: DIFFERENCES IN THE IMPELLER MAIN BLADE THICKNESS AT CONSTANT RADIUS OF 3-in

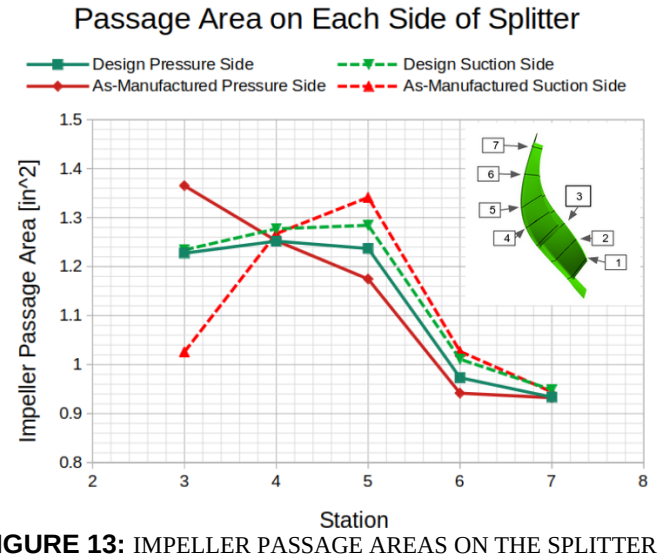

FIGURE 13: IMPELLER PASSAGE AREAS ON THE SPLITTER SUCTION SIDE (DASHED) AND PRESSURE SIDE (SOLID) FOR THE AS-MANUFACTURED (RED) AND DESIGN-INTENT (GREEN) MODELS

The discrepancies in the passage area on each side of the splitter for the As-Manufactured geometry indicate a possible source of the differences in the operating range shown in Figures 3 and 4. The As-Manufactured splitter suction side has a significantly lower area than the Design-Intent splitter suction side, causing it to ingest less flow than the corresponding Design-Intent passage. Progressing to the knee, this trend reverses. At Station 5, the splitter suction side has more area than the Design-Intent suction side. This results in less flow within the splitter suction side passage, which is then expanded to a greater extent, introducing the possibility of separation along the splitter suction side. The difference in passage inlet area is one physical change contributing to the change in the splitter incidence, along with the change to the splitter leading edge geometry.

5. PERFORMANCE EFFECTS OF GEOMETRIC DIFFERENCES

Each of these geometric differences was isolated and incorporated into the Design-Intent geometry as best as possible to determine the performance effect of each difference independently. To succinctly and quantitatively compare the performance effect of each geometric difference, a metric was created. This metric takes the ratio of the difference of the total pressure rise of the stage between the Design-Intent geometry and the isolated geometry difference to the difference of the total pressure rise of the Design-Intent geometry and the As-Manufactured geometry at a flow rate of 11 lbm/s. In other words, this metric will measure the percentage of the total pressure rise deficit between the Design-Intent and As-Manufactured geometries that is explained by each individual geometric difference. This metric will be evaluated at the design point for all hybrid geometry described in sections 5.1-5.4.

To evaluate each geometric difference in an isolated manner, the Design-Intent geometry was modified to incorporate individual differences at a time. These modified sections were then meshed and simulated using the same settings as the previous simulations. The mesh sensitivity study was not repeated for each configuration as the current mesh settings had been found to be converged for the As-Manufactured and Design-Intent geometries Thus, any effects observed are solely due to the geometry difference being studied rather than mesh and solver changes. It should be noted that the following simulations did not attempt to run the speedline all the way to numerical stall. Rather the speedlines were generated to develop an understanding of the changes to the aerodynamic performance at design speed as well as at the peak efficiency operating conditions (design point) at the design speed as a result of the individual and coupled geometric differences between the As-Manufactured and Design-Intent geometries.

5.1 Effect of Fillets

To quantify the performance effect of the presence of fillets, fillets similar in size to those on the As-Manufactured geometry were added to the Design-Intent geometry, and the results of this new geometry were compared to both the As-Manufactured and Design-Intent simulations. Note that the As-Manufactured geometry sections were extracted from the CAD itself, and these sections contain the fillets present in the physically manufactured hardware. Unfortunately, the specific radii and curvature of the fillets in the As-Manufactured sections were not readily available. So, an iterative approach was taken to mirror both the size and shape of the fillets in the As-Manufactured geometry onto the Design-Intent geometry. The fillets were added using a variable-radius fillet generation tool available for meshes generated by Code Wand. This tool enabled the specification of both radius and aspect ratio of the fillets at six independent locations along the airfoil. These locations were near the leading edge, mid chord, and near the trailing edge on both the pressure and suction sides of the airfoil. Because the impeller main blade and splitter are joined in the same mesh, the exact same fillets were applied to both the impeller and splitter. In the As-Manufactured geometry, there were some slight differences in the fillets on the impeller main blade and splitter. A qualitative approach was taken to create fillets that match both blades as best as possible, but they do not exactly replicate the fillets present in the As-Manufactured geometry. However, the fillets added to the Design-Intent geometry are similar enough to give a good approximation of the effect of adding the As-Manufactured fillets to the Design-Intent geometry. The results of this iterative approach can be seen in Figure 14, in comparison to the As-Manufactured fillets.

With the Design-Intent geometry containing fillets, the analysis was performed. The results of this modeling effort can be seen in Figure 15. The effect of the fillets on the performance of the Design-Intent geometry is negligible, as anticipated. The total pressure ratio decreased by only 0.0196, and according to this procedure, approximately 8% of the difference in TPR between the Design-Intent and As-Manufactured geometry at the design point is attributable to the presence of the fillets.

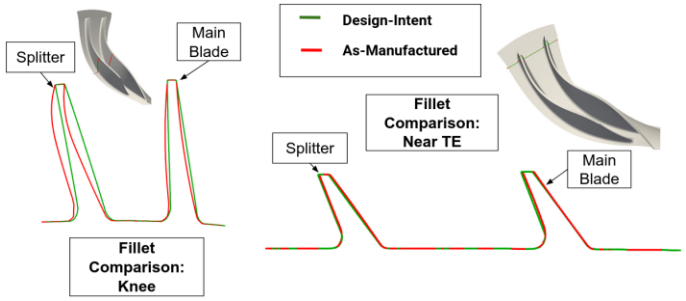

FIGURE 14: FILLETS ADDED TO DESIGN-INTENT GEOMETRY

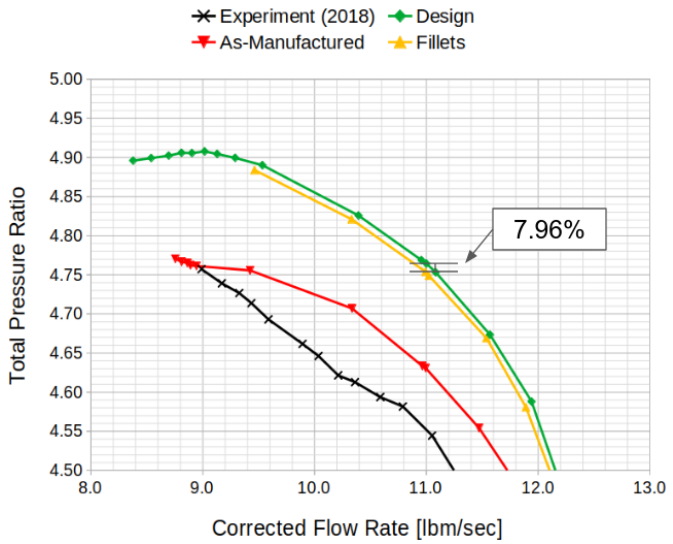

FIGURE 15: PERFORMANCE EFFECT OF THE PRESENCE OF FILLETS

5.2 Effect of Trailing-Edge Radius

To quantify the effect of the exit radial-coordinate differences, the Design-Intent geometry's impeller exit radius was reduced to match the As-Manufactured geometry's impeller exit radius. A linear interpolation of the As-Manufactured TE radius was taken, excluding the region affected by the cutoff fillets. The result of this modification can be seen in Figure 16. Note that this image shows the same trailing edge difference as Figure 9, but is zoomed in on the vertical axis.

Each of these methods were applied to both the impeller main blade and the splitter blade of the Design-Intent geometries, matching the corresponding blade in the As-Manufactured geometry. While performing the reduction of the Design-Intent trailing edge radius, care was taken to maintain the overall shape of the trailing edge of each section modified. Points were selected on the suction side and pressure side of the Design-Intent geometry near the trailing edge for each span, and relative positioning vectors between these points and the nearest adjacent

point were calculated. This relative positioning vector was then scaled such that the radial component of the relative positioning vector was reduced by the amount specified by the uniform shift or linear fit described previously in this section. All subsequent relative positioning vectors between the shifted point and the trailing edge were not modified.

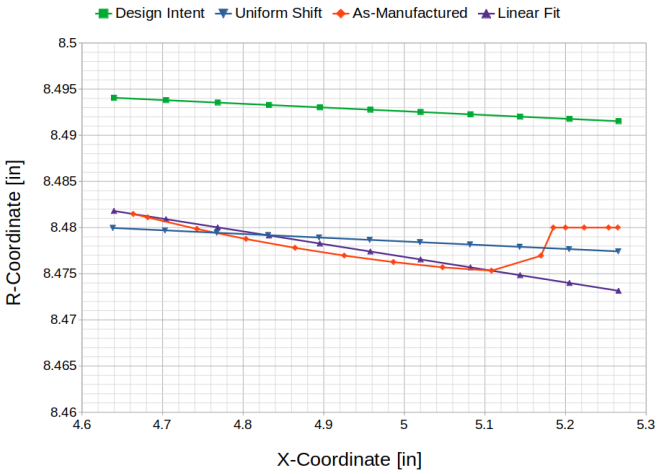

FIGURE 16: IMPELLER MAIN-BLADE TRAILING EDGE LINES BEFORE AND AFTER REDUCTION VIA UNIFORM SHIFT AND LINEAR FIT METHODOLOGIES

The analysis of this geometry yielded the following results, shown in Figure 17. The results show that there is a notable effect of the reduced trailing edge radius on the Design-Intent geometries' performance. The reduction of the trailing edge radius caused a reduction in the total pressure ratio of the Design-Intent stage of 0.0245. This value corresponds to 18.3% of the difference in pressure rise between the Design-Intent and As-Manufactured geometries.

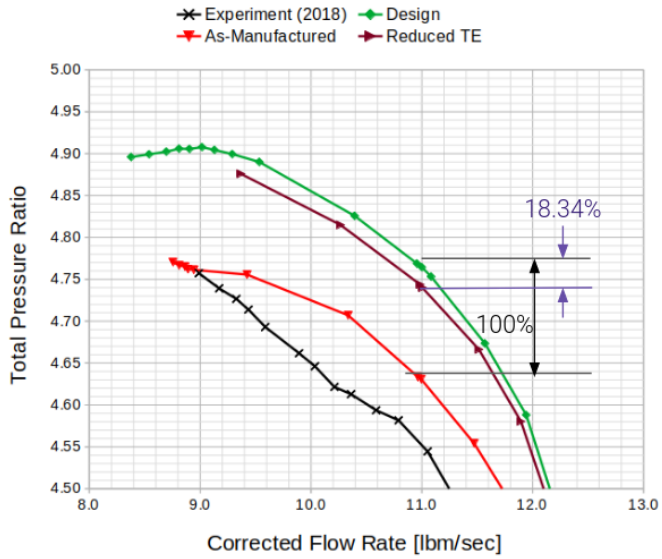

FIGURE 17: PERFORMANCE IMPACT OF REDUCTION OF TE RADIUS

5.3 Effect of Splitter Differences

One of the most striking differences between the Design-Intent and As-Manufactured geometries occurs in the splitter leading edge geometry. There is a notable bow in the Design-Intent splitter leading edge geometry that is not present in the As-Manufactured splitter leading edge geometry. To model this difference, an initial approach was taken to circumferentially shift each section of the Design-Intent splitter sections to match the As-Manufactured splitter leading edge. However, by doing this, the entire camber line of the Design-Intent geometry will change to be some combination of the Design-Intent camber line and the As-Manufactured camber line. Due to concerns that this model would not accurately capture the desired geometrical difference, or introduce new variables into the investigation, the decision was made to investigate the As-Manufactured splitter geometry paired with the Design-Intent impeller main blade. This combined geometry can be seen in Figure 18. One notable effect of this decision is that this geometry will not fully isolate differences in the splitter leading edge. This new model will capture the effects of the changes to the splitter leading edge, the presence of fillets on the splitter, and the reduced trailing edge on the splitter. The results of the analysis of this geometry can be seen in Figure 19.

The changes to the splitter geometry have a much greater effect than previous geometrical differences investigated. By including the As-Manufactured splitter with the Design-Intent impeller main blade, a reduction of the total pressure ratio of the stage of 0.0614 was found. This corresponds to 46.0% of the total difference in total pressure ratio seen between the Design-Intent and As-Manufactured geometries.

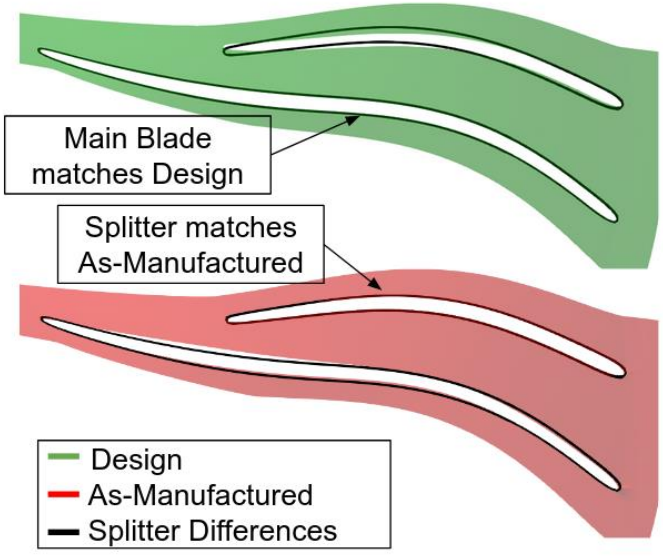

FIGURE 18: SPLITTER DIFFERENCES GEOMETRY

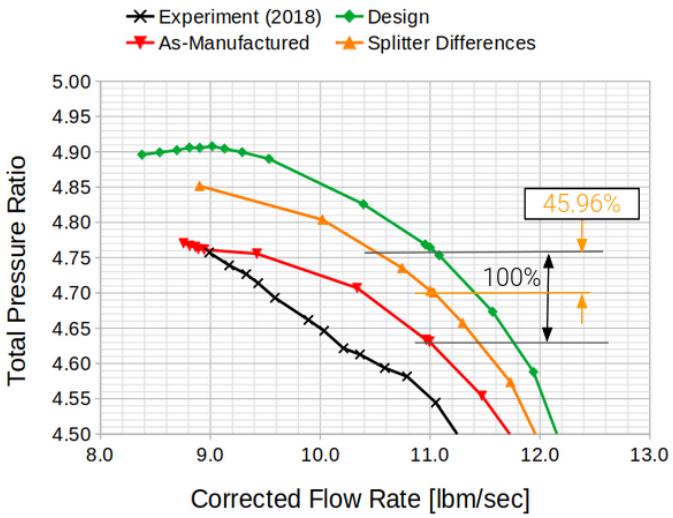

FIGURE 19: SPLITTER DIFFERENCES PERFORMANCE IMPACT

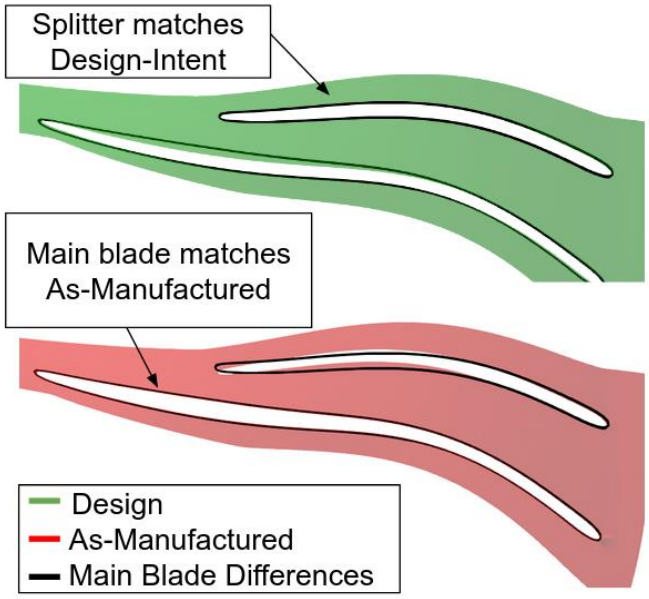

FIGURE 20: MAIN BLADE DIFFERENCES GEOMETRY

5.4 Effect of Main Blade Differences

Similar to the investigation into the differences in the splitter, it was determined that it would not be possible to modify the Design-Intent impeller main blade to mimic the As-Manufactured main blade thickness without introducing new variables into the investigation. For this reason, the decision was made to capture the effects of the differences in the main blades by replacing the Design-Intent main blade with the As-Manufactured main blade in a model containing the Design-Intent splitter. This combined geometry can be seen in Figure 20.

Once again, this geometry will capture the effects of fillets on the main blade and a reduced trailing edge on the main blade in addition to the change to the thickness of the main blade from the Design-Intent geometry to the As-Manufactured geometry. The results of the combined As-Manufactured main blade with the Design-Intent splitter can be seen below in Figure 21.

The Main-Blade Differences model shows a significant effect on the overall performance of the HECC. The pressure ratio of the stage was reduced by 0.033, which is 24.70% of the overall pressure ratio decrease between the Design-Intent and As-Manufactured geometries at 11 lbm/s of inlet corrected flow through the machine.

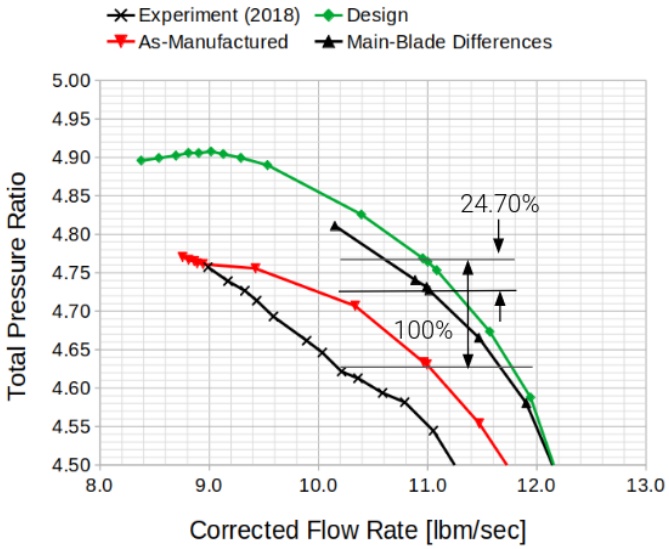

FIGURE 21: MAIN BLADE DIFFERENCES PERFORMANCE IMPACT

5.5 Summary of Effects of Geometric Differences

It was determined that each geometric difference found between the As-Manufactured and Design-Intent geometry plays some role in the overall performance degradation of the As-Manufactured HECC vaneless configuration. The presence of fillets played a minor role compared to the others. The reduction of the trailing edge radius reduces the total amount of work done by the machine and the pressure rise across the impeller, but it does not impact the efficiency of the HECC. It was identified in the loading profiles that a positive incidence on the splitter in the As-Manufactured geometry is the most notable driver of performance deficit in the As-Manufactured geometry. Figures 22.A and 22.B show similar loading profiles for each of the

geometric difference investigation cases. The positive incidence cannot be fully attributed to one single geometric difference, as both the changes to the main blade and the changes to the splitter each affect the incidence of the splitter. The presence of fillets and the reduction of the trailing edge radius do not have a noticeable impact on the loading of the impeller. Figure 22.A indicates that the majority of the reduction in work input of the main blade near 30% of the meridional distance can be attributed to differences in the main blade, but the differences in the splitter cause a small reduction in the same area. Similarly, Figure 22.B shows that the large overspeed on the splitter leading edge occurs when the splitter differences alone are considered, but a smaller overspeed does occur when the main blade differences are modeled. Additionally, a loss in work input of the splitter blade can be seen in the As-Manufactured splitter and the Splitter Differences configuration, but not in the other geometric modification configurations. The positive incidence and low momentum region behind it are not due to a single change to a geometric parameter – they are caused by multiple geometric differences.

A performance metric was used to evaluate the relative impact of each geometric difference at 11 lbm/s of corrected flowrate, and a summary of the findings can be seen in Figure 23.

Another key observation is the importance of the coupling effects between each of the geometric differences. None of the geometric differences by themselves account for the full drop in pressurization that was observed by themselves. Rather it's the cumulative impact of one geometric difference interacting with another that result in the drop. Take for example the splitter blade LE differences and the main blade thickness differences. The splitter blade differences do account for the largest share of the pressurization drop out of all four differences explored. However, it still does not account for all additional losses present in the As-Manufactured geometry. The splitter blade LE differences are further aggravated by the increased thickness of the main blade. This would bring the splitter blade LE even closer to the main blade and decrease the area even further. Thus, the coupling would intensify the mechanisms that consequently lead to the low momentum regions observed.

Moreover, the mixed geometry simulations incorporated the fillets and TE exit radius differences for the main or splitter blade being evaluated. Even though these were included and as a sum of both simulations all the geometric differences were explored, they do not add up to the drop observed in the As-Manufactured geometry (Figure 24). Rather, 29% of the pressurization loss is still unaccounted for. This difference is in part due to the Design-Intent portion of the mixed geometry not including the fillets and the change in TE exit radius. Nonetheless, as was shown before, these do not account for everything. Thus, it was observed that all these geometric differences interacting together are required to induce the observed pressure drop from Design-Intent to As-Manufactured.

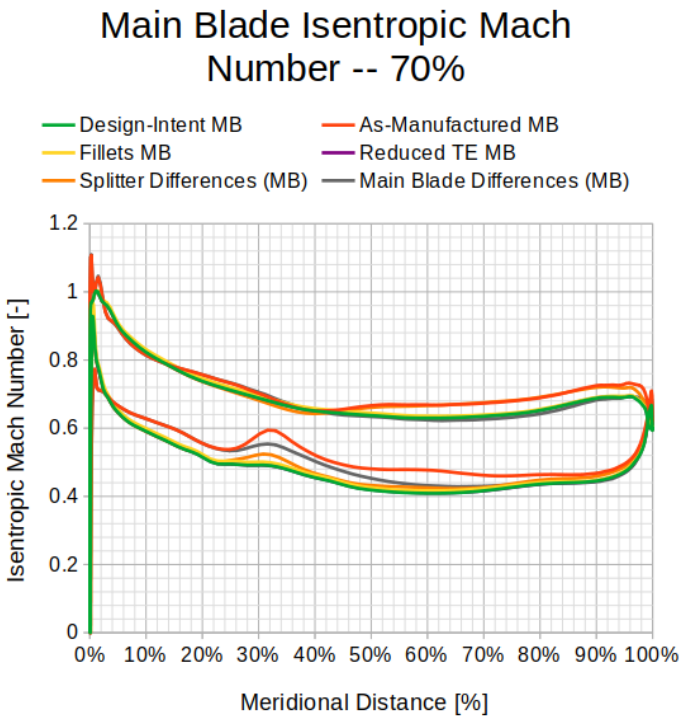

FIGURE 22.A: ISENTROPIC MACH NUMBER LOADING FOR THE IMPELLER MAIN BLADE OF EACH GEOMETRIC DIFFERENCE INVESTIGATION CASE

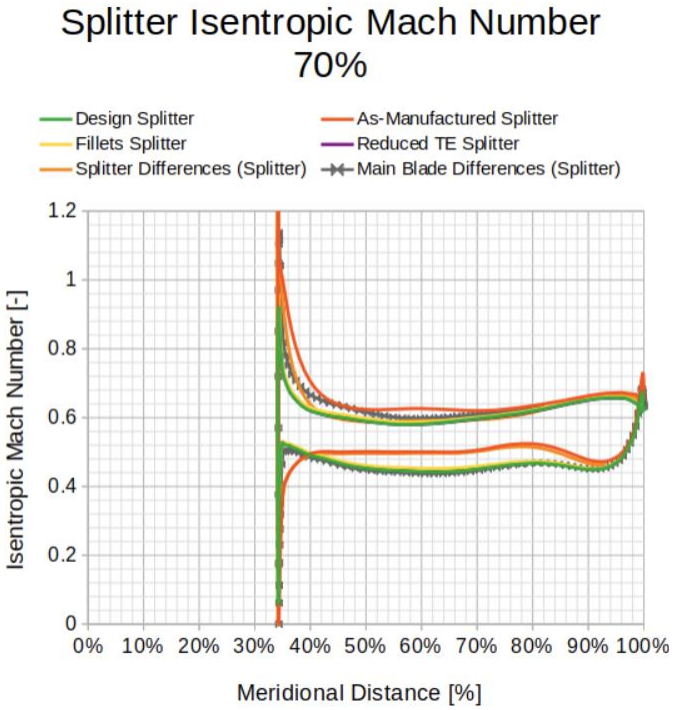

FIGURE 22.B: ISENTROPIC MACH NUMBER LOADING FOR THE IMPELLER SPLITTER BLADE OF EACH GEOMETRIC DIFFERENCE INVESTIGATION CASE

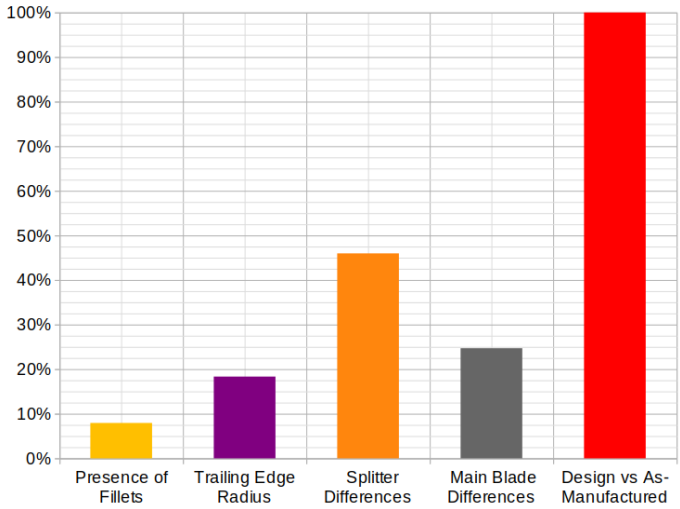

FIGURE 23: COMPARISON OF GEOMETRIC DIFFERENCES PERFORMANCE EFFECTS

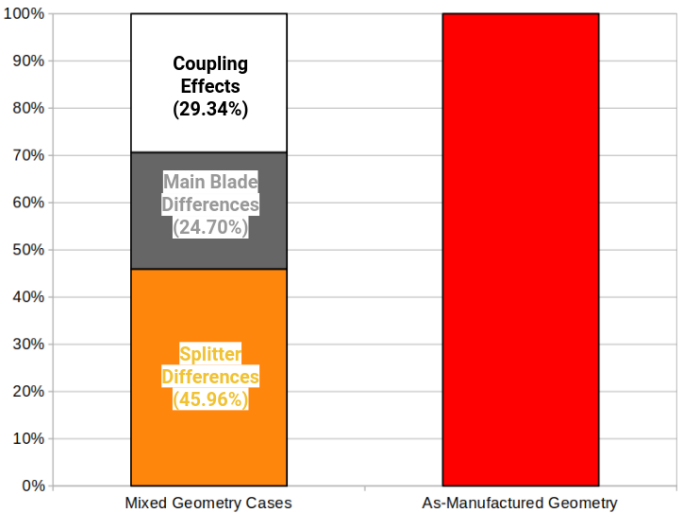

FIGURE 24: RELATIVE IMPACT OF COUPLING EFFECTS VS INDIVIDUAL BLADE DIFFERENCE CASES

6. CONCLUSION

Numerous models were developed to analyze performance of the High Efficiency Centrifugal Compressor impeller. The two initial models, termed As-Manufactured and Design-Intent, resulted in significant and surprising differences in the predicted total pressure ratio and efficiency of the impeller and vaneless diffuser configuration, with the Design-Intent model having improved performance relative to the As-Manufactured model. The cause of the differences was determined to be substantial differences in the impeller geometry between the two models, with the Design-Intent geometry being pulled from the HECC design report [7] and the As-Manufactured geometry being extracted from the solid model of the impeller. The solid model was verified to accurately reflect the physical geometry of the impeller in Part 1.

The major geometric differences between the two models were categorized into the presence/absence of fillets, the trailing edge radius, and the splitter and main blade variations. Each difference was meticulously incorporated into the Design-Intent geometry with the goal of determining the greatest contributor to the performance difference between the two models. The splitter blade differences and main blade differences contributed the most, followed by the trailing edge radius, and finally the fillets. Some allowance for coupling effects must be made, but the breakdown of the major contributors to the difference in performance was completed to the greatest level of rigor possible. The differences in the geometry noted here are greater than what could be expected or accounted for in cold-to-hot transformation procedures.

The ultimate finding from this work is that the Design-Intent HECC impeller geometry is not the same as the physical hardware that was built and tested at the NASA Glenn Research Center. The differences between the published geometry and the physical hardware are likely major contributors to the consistent differences in performance and aerodynamics observed between numerical models of the HECC and those measured in the experiment. Additional simulations by the community are recommended to verify the findings of the present work, as well as the completion of a cold-to-hot transformation of the As-Manufactured geometry to gain a more accurate representation of the physical geometry at design conditions.

REFERENCES

[1] Whitfield, A., and Baines, N. C., 1990, *Design of Radial Turbomachines*, Longman Scientific & Technical; Wiley, Harlow, Essex, England; New York, NY.

[2] Gooding, W. J., 2020, “Unsteady Diffuser Flow in an Aeroengine Centrifugal Compressor,” Dissertation, Purdue University.

[3] Greitzer, E. M., Tan, C. S., and Graf, M. B., 2007, *Internal Flow: Concepts and Applications*, Cambridge University Press, New York.

[4] Kamdar, N., Lou, F., and Key, N. L., 2021, “Details of Shrouded Stator Hub Cavity Flow in a Multi-Stage Axial Compressor Part 1: Interactions With the Primary Flow,” p. 12.

[5] Kamdar, N., Lou, F., and Key, N. L., 2021, “Details of Shrouded Stator Hub Cavity Flow in a Multistage Axial Compressor Part 2: Leakage Flow Characteristics in Stator Wells,” Journal of Engineering for Gas Turbines and Power, 144(011027).

[6] Wellborn, S. R., and Okiishi, T. H., 1999, “The Influence of Shrouded Stator Cavity Flows on Multistage Compressor Performance.”

[7] Medic, G., Sharma, O. P., Jongwook, J., Hardin, L. W., McCormick, D. C., Cousins, W. T., Lurie, E. A., Shabbir, A., Holley, B. M., and Van Slooten, P. R., 2017, *High Efficiency Centrifugal Compressor for Rotorcraft Applications*, E-18856-1.

[8] Holder, J. M., Turner, M., and Celestina, M., 2020, "Automated Turbomachinery Hot-to-Cold Transformation," *AIAA Scitech 2020 Forum*, American Institute of Aeronautics and Astronautics, Orlando, FL.

[9] Harrison, H. M., McNichols, E. O., and Blaha, M. R., 2023, "NASA Small Engine Components Compressor Test Facility: High Efficiency Centrifugal Compressor Vaneless Diffuser and Transition Duct Configurations," American Society of Mechanical Engineers Digital Collection.

[10] Harrison, H. M., 2022, "NASA HECC Data Archive," NASA [Online]. Available: https://storage.googleapis.com/hecc-data/NASA-HECC-Data-Archive.zip.

[11] Childs, P.R.N, and Noronha, M.B, "The Impact of Machining Techniques on Centrifugal Compressor Impeller Performance", Orlando, FL, June 2-5, 1997.97-GT-456

[12] Ni, R. H., 1982, "A Multiple-Grid Scheme for Solving the Euler Equations", AIAA 81-1025R